Theoretical search for high-performance thermoelectric donor-acceptor copolymers: the role of super-exchange couplings

Xue Yong[a], Gang Wu[a†], Wen Shi[a], Zicong Marvin Wong[a], Tianqi Deng[a], Qiang Zhu[c], Xiaoping Yang[e], Jian-Sheng Wang[b], Jianwei Xu[c,d], and Shuo-Wang Yang*[a]

a. Institute of High Performance Computing, Agency for Science, Technology and Research, 1 Fusionopolis Way, #16-16 Connexis, Singapore 138632
b. Department of Physics, Faculty of Science, National University of Singapore, 2 Science Drive 3, Singapore 117551
c. Institute of Materials Research and Engineering (IMRE), Agency of Science, Technology and Research (A*STAR), 2 Fusionopolis Way, Innovis, Singapore 138634, Singapore
d. Department of Chemistry, National University of Singapore, 3 Science Drive 3, Singapore 117543, Singapore
e. Anhui Province Key Laboratory of Condensed Matter Physics at Extreme Conditions, High Magnetic Field Laboratory, Chinese Academy of Sciences, Hefei 230031, China
† Corresponding author. Email: wug@ihpc.a-star.edu.sg
* Corresponding author. Email: yangsw@ihpc.a-star.edu.sg

Table of Contents

Section I.

Selection of coplanar model:

In small molecular gas phase, there is small torsions of 5-15 degrees between D and A fragments. However, the torsion angle in the crystalline form reduces to + /-5 ° due to the interaction between chains and symmetric packing.[1,2] Moreover, the coplanar configuration has been suggested in other theoretical and experimental work.[3,4] Therefore, to mimic the possible "planner form", we have used co-planner structures throughout our simulations. In order to further quantify the influence of the torsion angle, we perform additional calculations on two representative D-A models as shown in Figure S1a. The optimized model on the left has a torsion angle of 18° and the other is a coplanar structure. Our new computational results reveal that the two polymers have identical band structures and similar deformation constants: 10.0 eV vs. 8.5 eV, and elastic constants: 2.08×10^{-7} J m^{-1} vs. 1.47×10^{-7} J m^{-1}. Within the framework of deformation potential theory, the relaxation time is inversely related to the electron-phonon scattering matrix element $|M|^2 = k_{\mathrm{B}}\mathrm{T}E_1^2/C_{ii}$. For the two models, E_1^2/C_{ii} are calculated to be 0.770 and 0.787 eV Å, respectively, which means that the relaxation time can hardly be affected by the torsion. Therefore, the small twist only has minor effect on the electronic and final TE properties.

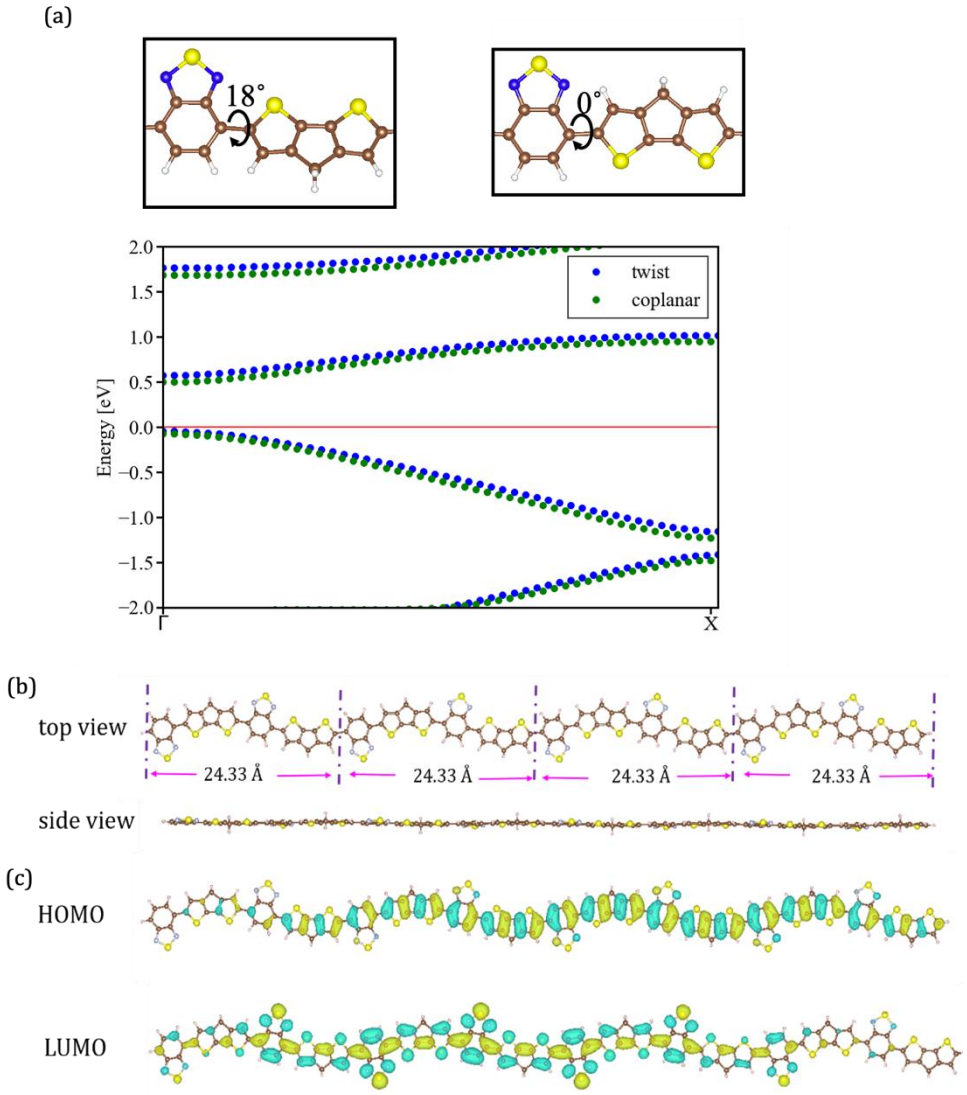

Figure S1: (a) Comparison the geometrical and band structure of the coplanar model with a model of ~ 15 ° torsion angle. (b)Optimized structure of tetramer and (c) the charge distributions of the highest-occupied-molecular-orbitals (HOMO) and lowest-unoccupied-molecular-orbitals (LUMO) of **BTCDT**

Selection of DFT functionals

We optimized the tetramer of **BTCDT** (Fig. S1) using M06 exchange-correlation functional[5] implemented in Gaussian 16 program[6] and 6-311+G(d,p) basis set for C, S, N, and H atoms. The acceptor BT units were constructed antiparallel along the oligomer backbone[2] thus the repeating unit consist of two donor units and two acceptor units. The optimized tetramer is found to be planar.

The length of the donor-acceptor unit is computed to be 24.33 Å, which is consistent with GIWAXS analysis (23.60 Å).[7]

PBE, B3LYP[8] and HSE06 and PBE0 with the Grimme's DFT-D3 van der Waals dispersion corrections have been evaluated for the band structure calculations for BTCDT. For the ease of computation, we used a short unit of one acceptor and one donor fragment to evaluate the functionals. The PBE, HSE06, B3LYP and PBE0 results are analogous which show a semiconducting band structure (Fig. S2). The valence and conduction bands have similar band width; however, the band gaps are fairly different. BTCDT polymer was found to exhibit an optical band gap around 1.4 eV and 1.75 eV.[9,10] Thus, DFT tends to underestimate the band gap. However, the electrical conductivity and Seebeck coefficient from PBE and PBE0 are identical (See Section III for details). Considering our main goal to be the understanding of the intrinsic TE properties and to achieve a balance between computational cost and accuracy, the PBE functional is therefore used to compute the electronic properties.

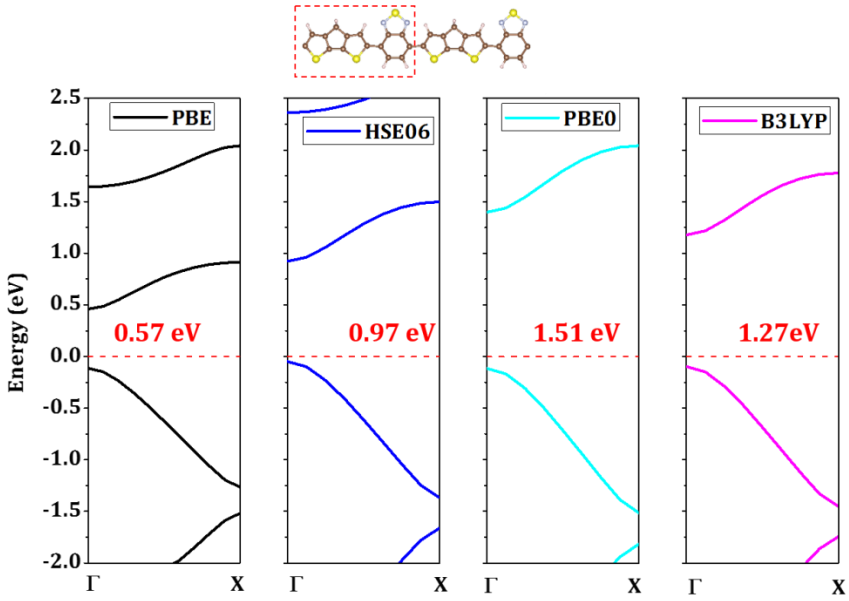

Figure S2: Band structures of **BTCDT** (top) obtained from different functionals including PBE, HSE06, PBE0, and B3LYP.

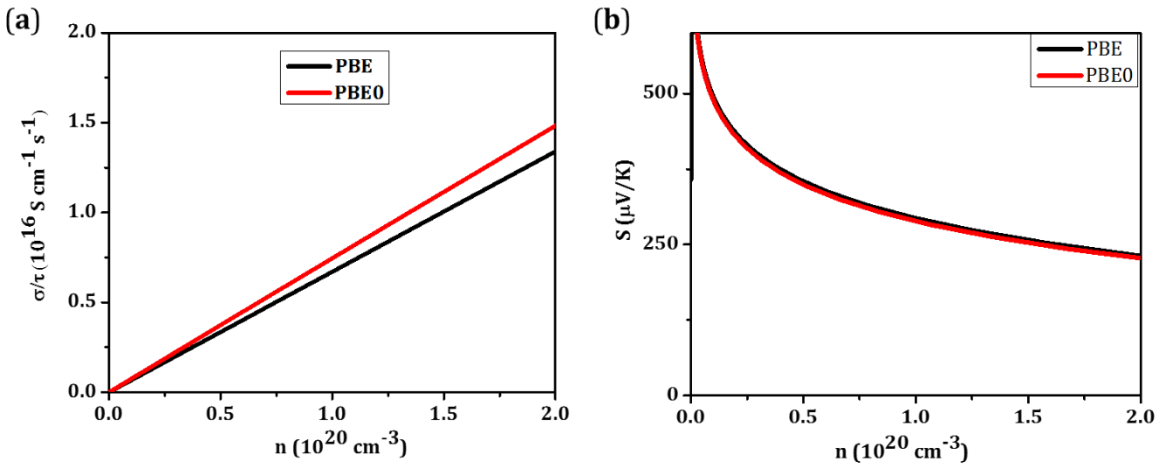

Figure S3: Computed σ/τ and S of **BTCDT** using PBE and PBE0 functional.

The σ/τ and Seebeck coefficient of **BTCDT** are computed by solving the constant time Boltzmann transport equations as implemented in BoltzTraP program.[11,12] At carrier concentrations up to 2.0 × 10^{20} cm^{-3}, the Seebeck coefficients computed from different functionals are identical. The σ/τ computed from different functionals are identical at lower carrier concentrations (less than 0.5 × 10^{20} cm^{-3}) and deviate slightly from 0.5 × 10^{20} cm^{-3} to 2.0 × 10^{20} cm^{-3}. The derived hole mobility μ/τ is 4.179 × 10^{14} cm^2 V^{-1} s^{-2}. Since the experimental mobility is reported to be 100 cm^2 V^{-1} s^{-2} for a fluoridated analog, the relaxation time is fitted to be 2.93 × 10^{-15} s.

Section II.

Tight-binding model

Here we present a simple two-level tight-binding model to uncover the key factors determining the deformation potential constant.

The second quantization Hamiltonian of the model system can be written as

$$H = \varepsilon_d a_d^\dagger a_d + \varepsilon_a a_a^\dagger a_a + \frac{t_{da}}{2} a_d^\dagger a_a + \frac{t_{da}^*}{2} a_a^\dagger a_d,$$

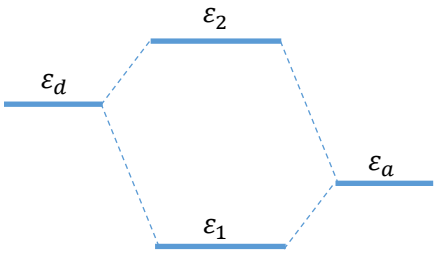

where $a_{a,d}^\dagger$ and $a_{a,d}$ are creation and annihilation operators on *acceptor* and *donor* segments, respectively. ε_d and ε_a are the corresponding on-site energies. t_{da} is the hopping parameter for the hopping between the two segments, and it is a function of the distance between the orbital centers of the two segments, r. Without loss of generality, we can assume t_{ad} to be a real number, thus $t_{ad} = t_{ad}^*$.

Furthermore, we can write the final wave function of the two-level system formally as

$$|\Psi\rangle = c_d|\phi_d\rangle + c_a|\phi_a\rangle,$$

where $|\phi_d\rangle$ and $|\phi_a\rangle$ are orthogonal molecular orbitals at *donor* and *acceptor* sites, respectively, and c_d and c_a are the corresponding expansion coefficients, respectively.

It is more convenient to express the eigen problem in matrix form as

$$\begin{bmatrix} \varepsilon_d & \frac{1}{2}t_{da} \\ \frac{1}{2}t_{da} & \varepsilon_a \end{bmatrix} \begin{pmatrix} c_d \\ c_a \end{pmatrix} = \varepsilon \begin{pmatrix} c_d \\ c_a \end{pmatrix}.$$

It is easy to obtain the eigenvalues and the eigenfunctions as follows,

$$\varepsilon_1 = \frac{1}{2}\left[\varepsilon_d + \varepsilon_a - \sqrt{(\varepsilon_d - \varepsilon_a)^2 + t_{da}^2}\right],$$

$$u_1 = \begin{pmatrix} c_d \\ c_a \end{pmatrix}_1 = \frac{1}{A}\begin{pmatrix} \frac{1}{t_{da}}\left[\varepsilon_d - \varepsilon_a - \sqrt{(\varepsilon_d - \varepsilon_a)^2 + t_{da}^2}\right] \\ 1 \end{pmatrix};$$

$$\varepsilon_2 = \frac{1}{2}\left[\varepsilon_d + \varepsilon_a + \sqrt{(\varepsilon_d - \varepsilon_a)^2 + t_{da}^2}\right],$$

$$u_2 = \begin{pmatrix} c_d \\ c_a \end{pmatrix}_2 = \frac{1}{B}\begin{pmatrix} \frac{1}{t_{da}}\left[\varepsilon_d - \varepsilon_a + \sqrt{(\varepsilon_d - \varepsilon_a)^2 + t_{da}^2}\right] \\ 1 \end{pmatrix}.$$

Here prefactors A and B are introduced to ensure u_1 and u_2 are normalized vectors. It is convenient to introduce $\alpha = \frac{\varepsilon_d - \varepsilon_a}{t_{da}}$ and $\beta = \frac{1}{t_{da}}\sqrt{(\varepsilon_d - \varepsilon_a)^2 + t_{da}^2}$, thus $A = \sqrt{(\alpha - \beta)^2 + 1}$, $B = \sqrt{(\alpha + \beta)^2 + 1}$. A very useful relation reads $\beta^2 - \alpha^2 = 1$.

Size effect

Taking an *infinite quantum well* model, we can argue that the onsite energy of the segments can be written as $\varepsilon \propto \frac{1}{l^2}$, where l is the length of the segment. It is easily proven that $\frac{\partial \varepsilon}{\partial l} = -2\frac{\varepsilon}{l}$.

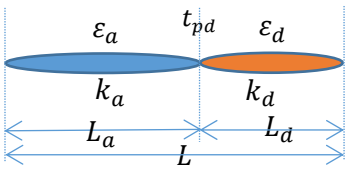

In addition, the hopping parameter t_{da} should depend on the distance between the fragmental orbitals. Taking Harrison scaling method, we have $t_{da} \propto \frac{4}{(L_d + L_a)^2}$. Still, we can prove that $\frac{\partial t_{da}}{\partial L} = -2\frac{t_{da}}{L}$.

In order to calculate the local deformation of each segment, we can assume that the local elastic constants of *donor* and *acceptor* segments are k_d and k_a, respectively, and the lengths of *donor* and *acceptor* regions are L_d and L_a, respectively, thus $L = L_d + L_a$. Because the stress in the system should be equal everywhere, we have

$$k_d\frac{\delta L_d}{L_d} = k_a\frac{\delta L_a}{L_a}, \text{ or } \delta L = \delta L_d + \delta L_a = \delta L_d\left(1 + \frac{k_d}{k_a}\frac{L_a}{L_d}\right) = \delta L_a\left(1 + \frac{k_a}{k_d}\frac{L_d}{L_a}\right).$$

Deformation potential constant

Now it is easy to derive the effective deformation potential constants for ε_1 and ε_2,

$$E_1 = \frac{d(\varepsilon_{1,2}-\bar{\varepsilon})}{dL/L} = \frac{L}{2}\left[\mp\frac{1}{2\sqrt{(\varepsilon_d-\varepsilon_a)^2+t_{da}^2}}\left(2(\varepsilon_d-\varepsilon_a)\left(\frac{\partial\varepsilon_d}{\partial L}-\frac{\partial\varepsilon_a}{\partial L}\right)+2t_{da}\frac{\partial t_{da}}{\partial L}\right)\right] =$$

$$\frac{L}{2}\left[\frac{\partial\varepsilon_d}{\partial L_d}\frac{1}{1+\frac{k_dL_a}{k_aL_d}}\left(\mp\frac{(\varepsilon_d-\varepsilon_a)}{\sqrt{(\varepsilon_d-\varepsilon_a)^2+t_{da}^2}}\right)+\frac{\partial\varepsilon_a}{\partial L_a}\frac{1}{1+\frac{k_aL_d}{k_dL_a}}\left(\pm\frac{(\varepsilon_d-\varepsilon_a)}{\sqrt{(\varepsilon_d-\varepsilon_a)^2+t_{da}^2}}\right)\mp\frac{t_{da}}{\sqrt{(\varepsilon_d-\varepsilon_a)^2+t_{da}^2}}\frac{\partial t_{da}}{\partial L}\right] =$$

$$-L\left[\frac{\varepsilon_dk_a}{k_aL_d+k_dL_a}\left(\mp\frac{(\varepsilon_d-\varepsilon_a)}{\sqrt{(\varepsilon_d-\varepsilon_a)^2+t_{da}^2}}\right)+\frac{\varepsilon_ak_d}{k_aL_d+k_dL_a}\left(\pm\frac{(\varepsilon_d-\varepsilon_a)}{\sqrt{(\varepsilon_d-\varepsilon_a)^2+t_{da}^2}}\right)\mp\frac{t_{da}}{\sqrt{(\varepsilon_d-\varepsilon_a)^2+t_{da}^2}}\frac{t_{da}}{L}\right] =$$

$$\pm L\left[\frac{\varepsilon_dk_a-\varepsilon_ak_d}{k_aL_d+k_dL_a}\left(\frac{\alpha}{\beta}\right)+\frac{1}{\beta}\frac{t_{da}}{L}\right].$$

Here $\bar{\varepsilon} = \frac{1}{2}(\varepsilon_1+\varepsilon_2)$ measures the position of Fermi level as the middle of the VBM and CBM.

If $k_d = k_a$, $E_1 = \pm\left[\frac{\alpha}{\beta}(\varepsilon_d-\varepsilon_a)+\frac{t_{da}}{\beta}\right] = \pm\sqrt{(\varepsilon_d-\varepsilon_a)^2+t_{da}^2}$.

Periodic system:

Above discussion can be further extended to infinite periodic system. Still assuming the hopping parameter between the p_z orbitals of the donor and acceptor segments is t, the only modification is to replace the hopping parameter t_{da} in previous derivations with $t_{da}^{\text{eff}} = te^{ik\pi} + (t)e^{-ik\pi} = 2t\cos k\pi$, where k is the wave vector in the first Brillouin zone in the unit of $\frac{1}{L}$, and L is the periodic length. Now the eigenvalue problem becomes

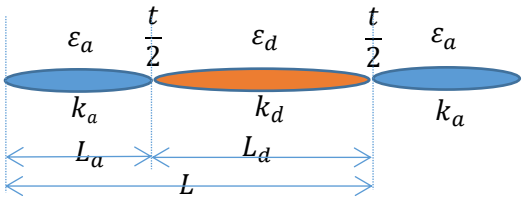

$$\begin{bmatrix} \varepsilon_d & t\cos k\pi \\ t\cos k\pi & \varepsilon_a \end{bmatrix}\begin{pmatrix} c_d \\ c_a \end{pmatrix} = \varepsilon\begin{pmatrix} c_d \\ c_a \end{pmatrix}.$$

Then the eigen-energies can be written as

$$\varepsilon_1 = \frac{1}{2}\left[\varepsilon_d + \varepsilon_a - \sqrt{(\varepsilon_d - \varepsilon_a)^2 + 4t^2\cos^2 k\pi}\right];$$

$$\varepsilon_2 = \frac{1}{2}\left[\varepsilon_d + \varepsilon_a + \sqrt{(\varepsilon_d - \varepsilon_a)^2 + 4t^2\cos^2 k\pi}\right].$$

Band folding

If two (flipped) repeated unit cells are connected to form a new unit cell, the Hamiltonian becomes

$$H = \begin{bmatrix} \varepsilon_d & te^{i\frac{\pi}{2}k} & 0 & te^{-i\frac{\pi}{2}k} \\ te^{-i\frac{\pi}{2}k} & \varepsilon_a & te^{i\frac{\pi}{2}k} & 0 \\ 0 & te^{-i\frac{\pi}{2}k} & \varepsilon_d & te^{i\frac{\pi}{2}k} \\ te^{i\frac{\pi}{2}k} & 0 & te^{-i\frac{\pi}{2}k} & \varepsilon_a \end{bmatrix},$$

then the eigenvalues become

$$\varepsilon_{1,2} = \frac{1}{2}\left[\varepsilon_d + \varepsilon_a \pm \sqrt{(\varepsilon_d - \varepsilon_a)^2 + 16t^2\cos^2\frac{k\pi}{2}}\right],$$

$$\varepsilon_{3,4} = \frac{1}{2}\left[\varepsilon_d + \varepsilon_a \pm \sqrt{(\varepsilon_d - \varepsilon_a)^2 + 16t^2\sin^2\frac{k\pi}{2}}\right].$$

Now the band edge appears at Γ point ($\sin\frac{k\pi}{2} = 0$). All the above discussions still hold.

Finite depth well

For finite depth well, we can assume the potential $V(x) = \begin{cases} -V_0, & |x| < l/2 \\ 0, & |x| > l/2 \end{cases}$. Here system size is l.

When $|x| > l/2$, $E = -\frac{\hbar^2\gamma^2}{2m}$, $\varphi(x) \propto e^{-|\gamma x|}$.

When $|x| < l/2$, $E = -V_0 + \frac{\hbar^2 k^2}{2m}$, $\varphi(x) \propto e^{\pm ikx}$.

Using the continuity of $\varphi(x)$ and $\varphi'(x)$ at $x = \pm\frac{l}{2}$, we can obtain $\frac{kl}{2}\tan\left(\frac{kl}{2}\right) = \frac{l}{2}\gamma$.

Now we can take the first derivate of the above equation against the system size l and obtain $\frac{\partial k}{\partial l}\left[\tan\frac{kl}{2}+\frac{kl}{2}\left(1+\tan^2\frac{kl}{2}\right)\right]+\frac{k^2}{2}\left(1+\tan^2\frac{kl}{2}\right)=\frac{\partial\gamma}{\partial l}$.
Using the relation between k, γ, and E, we can arrive at
$\frac{\partial E}{\partial l}=-\frac{2}{l}\frac{\hbar^2k^2}{2m}\frac{1}{1+\frac{1}{\frac{l}{2}\gamma}}$, or equivalently $\left(-\frac{1}{2}\right)\frac{l}{E+V_0}\frac{\partial(E+V_0)}{\partial l}=\frac{1}{1+\frac{1}{\gamma l/2}}\in(0,1)$.
γ itself is difficult to be solved, however, to the first order approximation, we can approximate the energy $E+V_0$ using the energy spectrum from the infinite depth well, namely, $E=-V_0+\frac{\hbar^2\pi^2}{2ml^2}n^2$, $n=1,2,3,\cdots$, thus $\gamma l=\sqrt{\frac{2mV_0l^2}{\hbar^2}-\pi^2n^2}$.

Long range hopping and SE coupling

Because the conduction and valence bands of the D-A polymers often show different bandwidths, and this difference stems from the interaction between the second neighbor inter-segment interactions, we have to consider this kind of interactions explicitly.
Now Hamiltonian becomes

$$H=\begin{bmatrix}\varepsilon_d & t_{ad}e^{i\frac{\pi}{2}k} & 2s_{dd}\cos k\pi & t_{ad}e^{-i\frac{\pi}{2}k}\\ t_{ad}e^{-i\frac{\pi}{2}k} & \varepsilon_a & t_{ad}e^{i\frac{\pi}{2}k} & 2s_{aa}\cos\ k\pi\\ 2s_{dd}\cos k\pi & t_{ad}e^{-i\frac{\pi}{2}k} & \varepsilon_d & t_{ad}e^{i\frac{\pi}{2}k}\\ t_{ad}e^{i\frac{\pi}{2}k} & 2s_{aa}\cos\ k\pi & t_{ad}e^{-i\frac{\pi}{2}k} & \varepsilon_a\end{bmatrix},$$

where s_d and s_a are second neighbor inter-segment hopping parameters.
Solving the eigen-problem and we can obtain

$$\varepsilon_{1,2}=\frac{1}{2}\left[\varepsilon_d+\varepsilon_a-(s_{aa}+s_{dd})\cos k\pi\pm\sqrt{(\varepsilon_d-\varepsilon_a-2(s_{dd}-s_{aa})\cos k\pi)^2+16{t_{ad}}^2\sin^2\frac{k\pi}{2}}\right],\qquad(1)$$

$$\varepsilon_{3,4}=\frac{1}{2}\left[\varepsilon_d+\varepsilon_a+(s_{aa}+s_{dd})\cos k\pi\pm\sqrt{(\varepsilon_d-\varepsilon_a-2(s_{dd}-s_{aa})\cos k\pi)^2+16t_{ad}^2\cos^2\frac{k\pi}{2}}\right].$$

(2)

The transfer integral t_{ad}, s_{aa}, and s_{dd} are obtained by solving the equations (1) and (2) where ε_1 , ε_2, ε_3, and ε_4 are taken from the DFT calculations. Finally, the SE couplings are computed with the as $SE=s_{aa}+s_{dd}$.

Some useful quantities:

a) Gap size: $E_g=|(\varepsilon_d-\varepsilon_a)-2(s_d-s_a)|$. (at Γ point)
b) Conduction band width: $E_b^c=\frac{1}{2}\left[\sqrt{E_g^2+16t^2}-E_g\right]+(s_d+s_a)$.

c) Valence band width: $E_b^v = \frac{1}{2}\left[\sqrt{E_g^2 + 16t^2} - E_g\right] - (s_d + s_a)$.

d) Effective mass at CBM: $m^{*,c} = \frac{4\hbar^2}{L^2}\frac{1}{\frac{2t^2}{E_g}+\frac{3s_a - s_d}{2}}$.

e) Effective mass at VBM: $m^{*,v} = \frac{4\hbar^2}{L^2}\frac{1}{\frac{2t^2}{E_g}-\frac{3s_a - s_d}{2}}$.

Some interesting relations can be observed from the above equations. We can easily obtain that the conduction band width E_b^c is an increasing linear function of $SE = s_d + s_a$. After assuming $s_a \sim s_d$, it can also be seen that the inversed effective mass at CBM is a linear function of SE. Although it is difficult to determine the relation between the energy gap E_g and SE, we can still get a rough estimation that they are linearly correlated. All these can be seen clearly from Fig. 3, and some of them has been observed in other publications[3].

Section III.

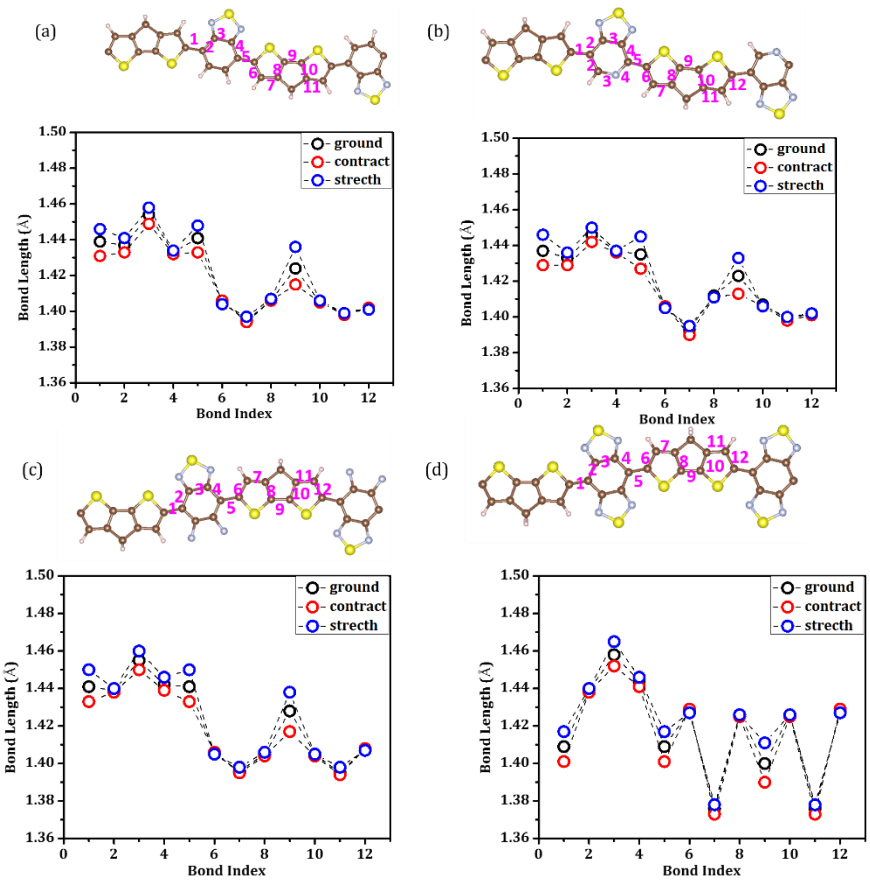

Figure S4: Bond length differences for (a) BTCDT, (b) PTCDT, (c) DFBTCDT, and (d) DBTCDT, and their corresponding optimized structures are shown above.

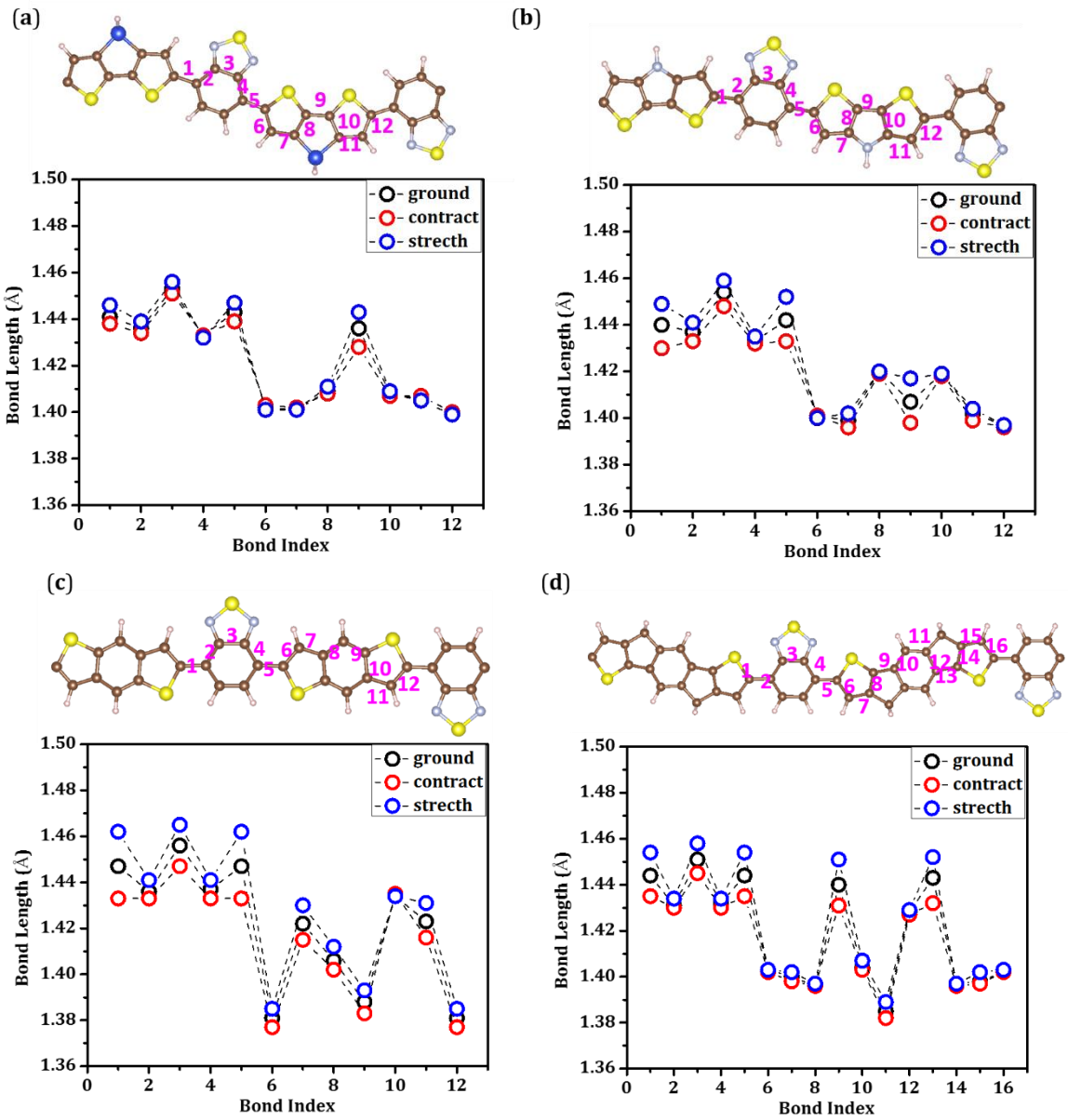

Figure S5: Bond length differences for (a) BTSiDT, (b) BTNDT, (c) BTBDT, and (d) BTIDT, and their corresponding optimized structures are shown above.

Table S1: The HOMO, LUMO, band gap E_g, SE couplings, and direct nearest couplings (t_{da}), Bader charge of the D-A polymers studied.

	HOMO/eV	LUMO/eV	E_g/eV	SE coupling /eV	t_{da}/eV	Bader charge /e
BTCDT	-4.20	-3.68	0.52	0.21	0.53	0.12
PTCDT	-4.38	-3.93	0.45	0.21	0.52	0.25
DFBTCDT	-4.42	-3.79	0.63	0.20	0.72	0.40
DBTCDT	-4.34	-4.10	0.24	0.26	0.42	0.48
BTSiDT	-4.44	-3.81	0.63	0.18	0.54	0.14
BTNDT	-4.17	-3.63	0.54	0.22	0.50	0.11
BTBDT	-4.78	-3.84	0.94	0.09	0.44	0.18
BTIDT	-4.23	-3.52	0.71	0.14	0.42	
***h*-CDT**				0.19	1.14	

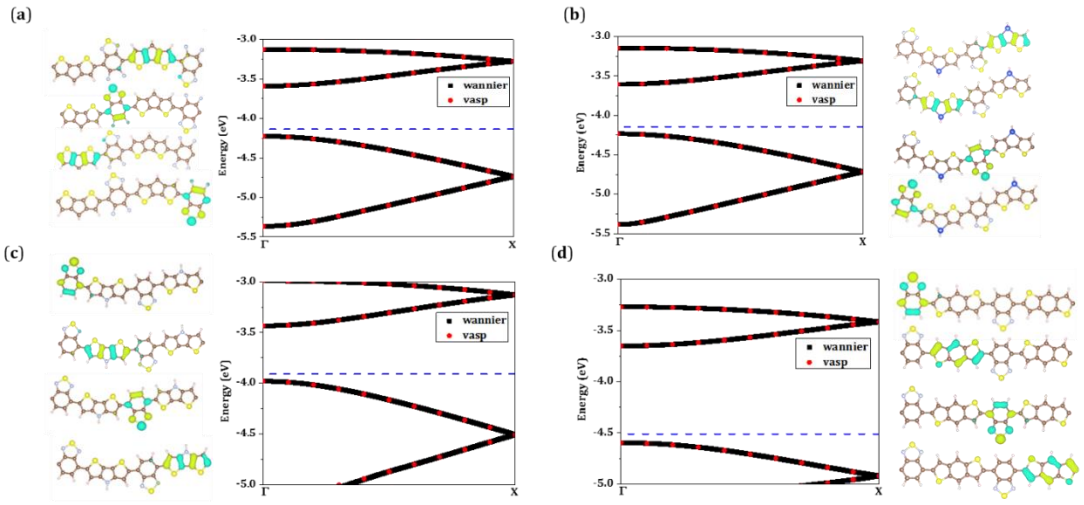

Figure S6: The band structures and corresponding Wannier function basis set localized on D and A fragment for (a) **DFBTCDT**, (b) **BTSiDT**, (c) **BTNDT**, and (d) **BTBDT**.

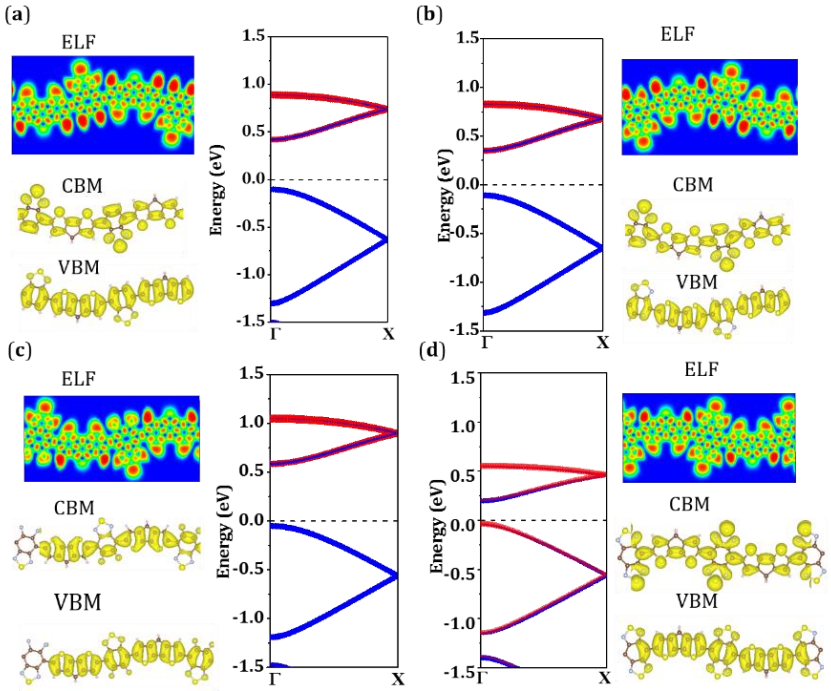

Figure S7: The ELF, VBM and CBM partial charge distributions, and band structures for (a) **BTCDT**, (b) **PTCDT**, (c) **DFBTCDT**, and (d) **DBTCDT**

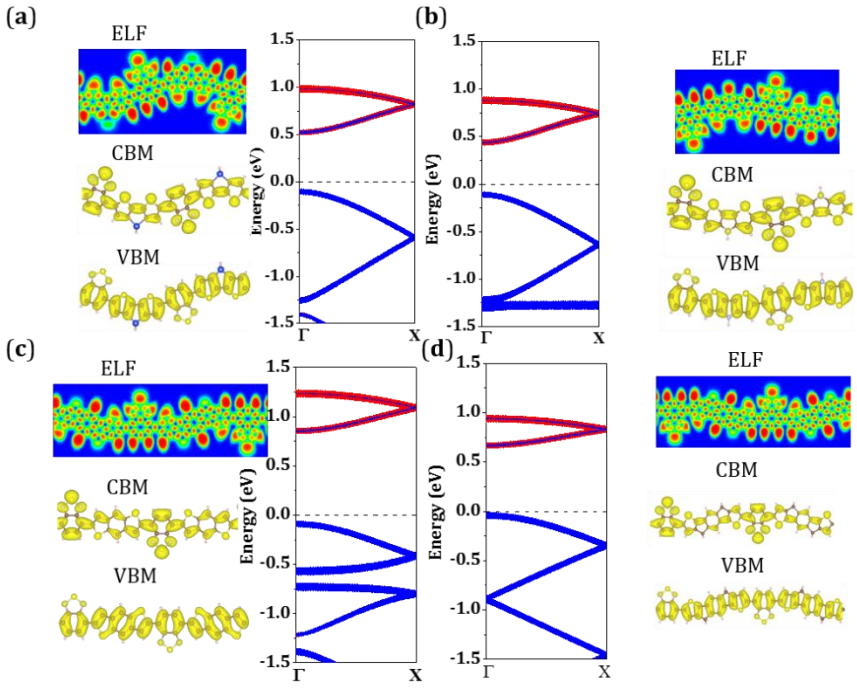

Figure S8: The ELF, VBM and CBM partial charge distributions, and band structures for (a) **BTSiDT**, (b) **BTNDT**, (c) **BTBDT**, and (d) **BTIDT**.

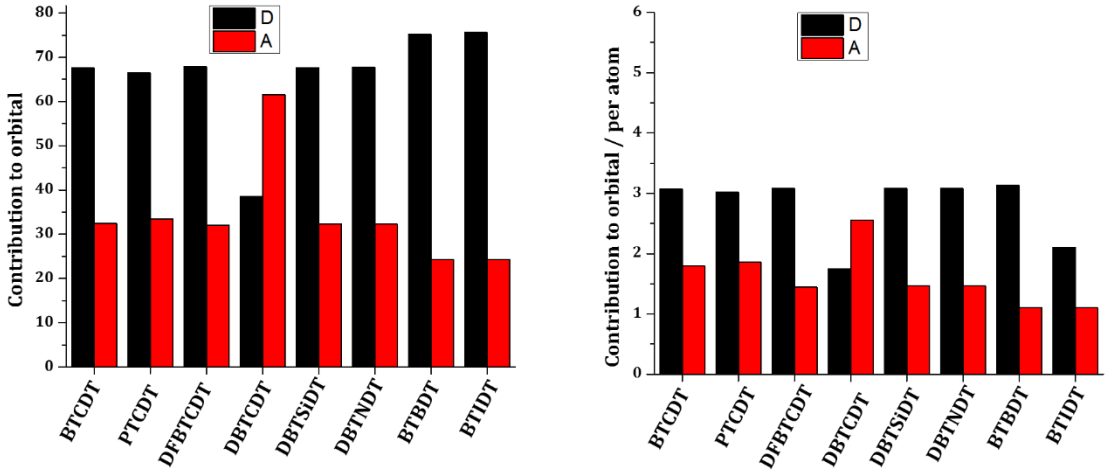

Figure S9: The contributions from D_p_z and A_p_z orbitals to the valance bands

Section IV.

The DP constant which describes the energy band shift due to the crystal lattice deformation is defined as $E_1 = \frac{\Delta E_{\mathrm{CB(VB)}}}{\Delta x/x_0}$. Here $\Delta E_{\mathrm{CB(VB)}}$ is the absolute position change of band edge with the lattice deformation in the crystal axis x direction (Figure S10b). The vacuum level, E_{vacuum} is

treated as the energy reference. We employ vacuum energy level calibration method[13] to calculate the absolute energy levels of valence/conduction band maximum/minimum (VBM/CBM), E_{VBM}/ E_{CBM}. The schematic illustration of the calibration method is displayed in Fig. S7. The electrostatic potential profiles along the crystal axis *z* direction were calculated from the offsets between the band edge positions and vacuum level estimation, namely $E_{CBM/VBM} = E^0_{CBM/VBM} - E_{vacuum}$, where $E^0_{CBM/VBM}$ is the uncalibrated CBM or VBM energy level.

The elastic constant, $\underline{C_{ii}}$ was calculated by stretching the unit cell along the crystal axis *x*-direction by ±0.5% and ± 1.0% and then fitting the total energy, *E* of deformed lattice concerning the dilation, $\Delta x/x_0$ via the formula $\frac{E-E_0}{x_0 yz} = \frac{C_{ii}}{2}\left(\frac{\Delta x}{x_0}\right)^2$. Figure S10a displays the fitting for C_{ii}.

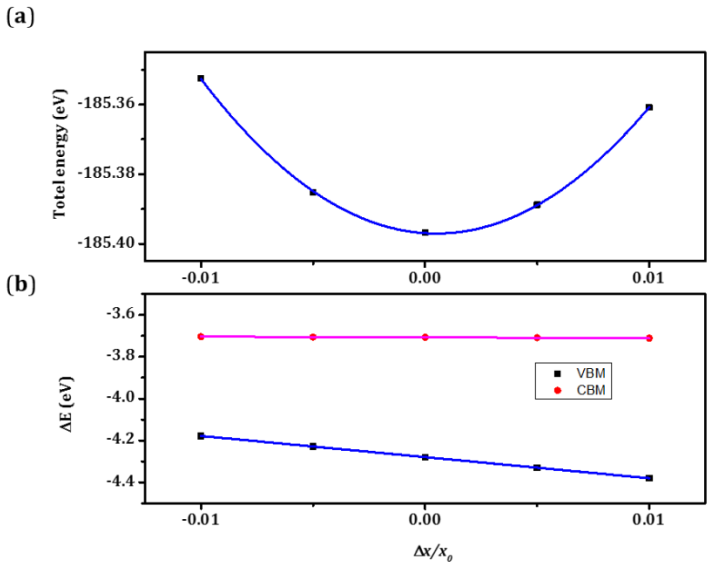

Figure S10: (a) The total energy with respect to dilations for **BTCDT** in the crystal axis *x* direction. The solid black lines are the parabolic fittings of data points. (b) The band energy shifts concerning dilations for **BTCDT** in the crystal axis *x* direction. The valence band maximum (VBM) (purple) and conduction band minimum (CBM) (blue) are used to obtain the DP constants of holes and electrons, respectively. The energies are all calibrated to the vacuum level during the lattice deformations. The solid lines are the linear fittings of data points.

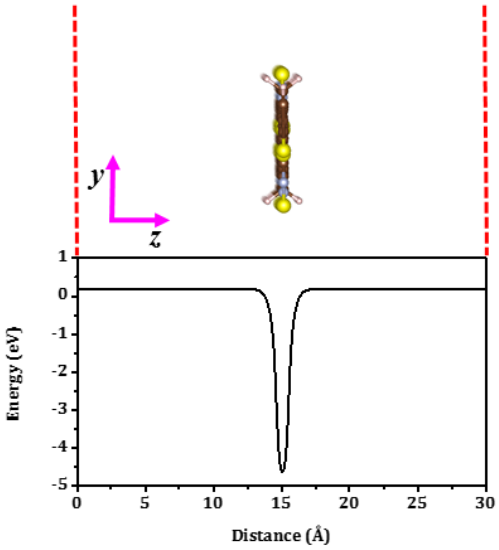

Figure S11: The schematic illustration of the calibration method: the electrostatic potential profiles for **BTCDT** in the crystal axis *z* direction.

Table S2: Changes in the site energy (fragmental orbital levels which comprise the valence band) in each D-A polymer upon a 1% lattice stretch.

	Ground*		0.1% tensile					
	E_{HOMO} (A)	E_{HOMO} (D)	E_{HOMO} (A)	E_{HOMO} (D)	E_{HOMO} (D)- E_{HOMO} (A)	Δref	Δrelative	100*(Δref + Δrelative)
BTCDT	-6.786	-5.368	-6.794	-5.406	1.419	0.022	0.030	5.29
PTCDT	-7.227	-5.341	-7.235	-5.383	1.886	0.024	0.034	5.823
DFBTCDT	-7.257	-5.362	-7.262	-5.407	1.895	0.025	0.039	6.435
DBTCDT	-6.337	-5.201	-6.34	-5.246	1.136	0.027	0.044	7.061
BTSiDT	-6.793	-5.618	-6.797	-5.637	1.175	0.011	0.015	2.612
BTNDT	-6.789	-5.340	-6.799	-5.384	1.448	0.027	0.034	6.108
BTBDT	-6.816	-5.647	-6.827	-5.663	1.169	0.013	0.005	1.918
BTIDT	-6.791	-5.193	-6.800	-5.249	1.598	0.033	0.047	8.00

[a] $D = E'_{\mathrm{HOMO}}(D) - E_{\mathrm{HOMO}}(D)$, [b] $A = E'_{\mathrm{HOMO}}(A) - E_{\mathrm{HOMO}}(A)$, [c] ref $= \frac{(D+A)}{2}$, [d] relative $= |D - A|$, *Ground: Ground-state before lattice stretch.

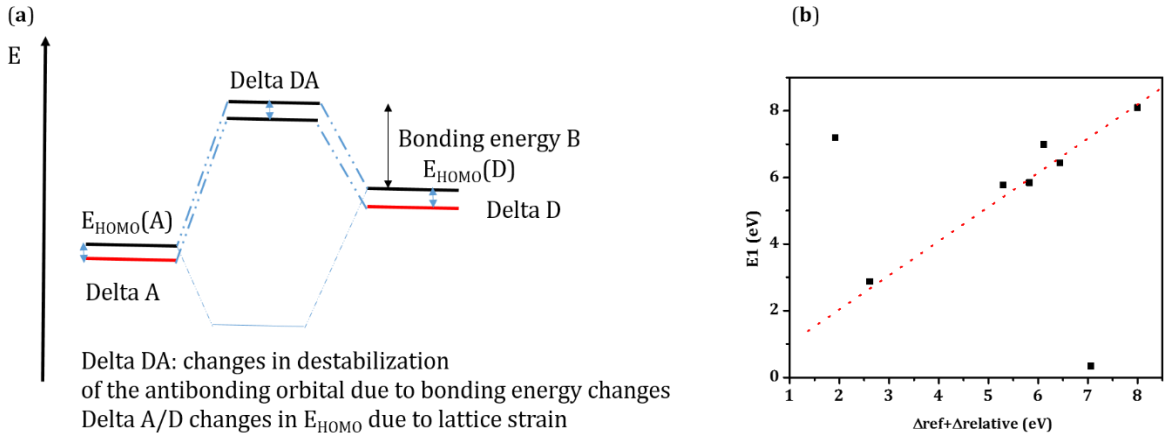

Figure S12: (a) Molecular orbital scheme of the donor acceptor interaction changes, under uniform lattice strain. (b) E_1 from DFT comparing with site energies changes from TB.

Table S3: The computed DP constants, elastic constants, power factor, Seebeck coefficients, electrical conductivity, mobility, and relaxation time for the D-A copolymers.

	E_1	c_{ii} (10^{-7} J m^{-1})	N_{opt} (10^{20} cm^{-3})	$(S^2\sigma)_{max}$ (10^{-3} W cm^{-1} K^{-2})	S (μV K^{-1})	σ (10^5 S cm^{-1})	Mobility (cm^2 V-1 s-1)	τ (ps)
BTCDT	5.78	1.12	2.73	1.41	173	0.471	879	42.42
PTCDT	5.84	1.11	2.66	2.08	177	0.662	993	51.56
DFBTCDT	6.43	1.26	1.69	0.77	190	0.212	749	45.48
DBTCDT	0.34	1.23	1.76	724	174	162	49200	1978
BTSiDT	2.87	0.64	1.74	1.29	190	0.359	1198	70.31
BTNDT	6.99	1.37	2.34	1.20	172	0.403	812	56.00
BTBDT	7.19	2.06	1.09	0.72	184	0.126	340	27.72
BTIDT	8.10	1.33	1.12	0.19	185	0.05	319	35.50

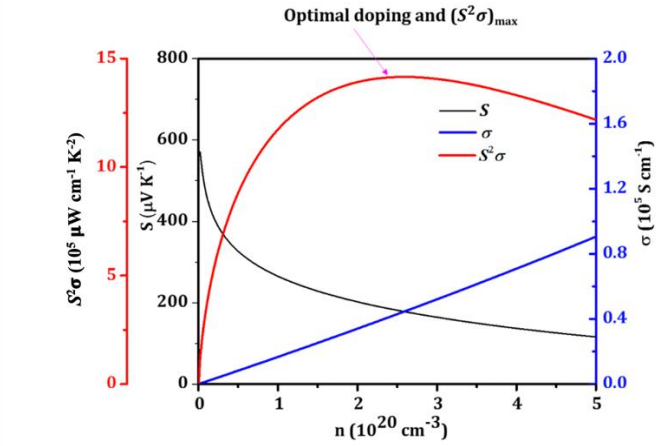

Figure S13: Variation of Seebeck coefficient, conductivity, and power factor with different carrier concentrations for **BTCDT** at room temperature.

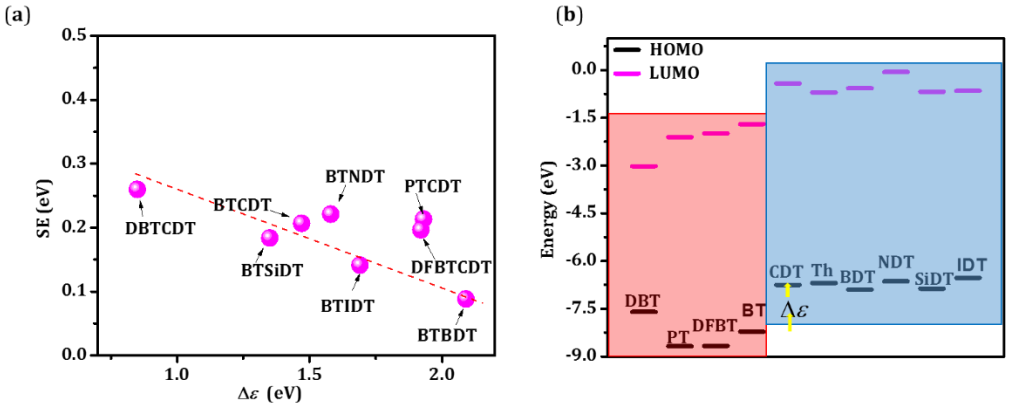

Figure S14: (a) Variation of SE couplings with respect to the energy difference between the frontier molecular orbitals between D and A moieties, (b) the energy level of the highest occupied molecular orbitals of D and A fragments.

The route to high TE power factor

The above results unravel strong SE coupling to play a key role in high-performance TE D-A copolymer. A strong SE coupling within the D-A copolymer results in small effective mass, small DP constant, and thus, weak electron-phonon coupling, large charge carrier relaxation time, and consequently, high mobility and high TE power factor. Further analysis reveals that SE couplings increase when there is a minimal energy difference ($\Delta\varepsilon = E_{\mathrm{HOMO}}(\mathrm{Donor}) - E_{\mathrm{HOMO}}(\mathrm{Acceptor})$) between the HOMOs of the acceptor and donor moiety (Figure S14a-b). For example, with respect to the same donor fragment (CDT), the $\Delta\varepsilon$ for DBT is 0.85 eV, whereas it is enhanced to 1.47 eV for BT, 1.93 eV for PT, and 1.92 eV for DFBT. The SE couplings, as given above, decrease from **DBTCDT** to **DFBTCDT** while the power factor increases from **DBTCDT** to **DFBTCDT**. In other words, SE couplings become stronger when there is appropriate frontier molecular orbital alignment

between the donor and acceptor moiety which agrees with our previous work that good molecular orbital alignment between the sub-building blocks leads to high TE power factor.[56] Thus a strategy to achieve a high power factor in D-A copolymer is to minimize the energy difference between the donor and acceptor moieties which bring forth strong SE coupling. Here we'd like to emphasize that our strategy only provides a feasible way to enhance the SE coupling. In the polymer, both direct coupling (t) and the SE determine the transport properties. Our results indicate that the direct coupling t of homopolymer is much larger than SE and dominating the transport properties. Thus, electronic properties of homo-polymers are mainly determined by the direct coupling. [10,11] For example, the *t* is 6 times of SE in *h*-CDT; while *t* is only 1.5~3 times of SE in the considered D-A polymer. And thus, SE coupling plays a more important role in determining the electronic properties of D-A polymers, which was also suggested in literatures[10,11]. In this sense, homopolymer and D-A copolymer should be treated separately, and our strategy should be applied for D-A polymers only, so that a large SE and modest direct coupling can be achieved simultaneously. In addition, this approach would be only applicable to semiconducting D-A copolymers where the HOMO and LUMO of the acceptors are lower than those of donors.

References

(1) Luo, C.; Kyaw, A. K. K.; Perez, L. A.; Patel, S.; Wang, M.; Grimm, B.; Bazan, G. C.; Kramer, E. J.; Heeger, A. J.; Kyaw, K. K.; Perez, L. A.; Patel, S.; Wang, M.; Grimm, B.; Bazan, G. C.; Kramer, E. J.; Heeger, A. J. General Strategy for Self-Assembly of Highly Oriented Nanocrystalline Semiconducting Polymers with High Mobility. *Nano Lett.* **2014**, *14* (5), 2764–2771. https://doi.org/10.1021/nl500758w.

(2) Niedzialek, D.; Lemaur, V.; Dudenko, D.; Shu, J.; Hansen, M. R.; Andreasen, J. W.; Pisula, W.; Müllen, K.; Cornil, J.; Beljonne, D. Probing the Relation Between Charge Transport and Supramolecular Organization Down to Ångström Resolution in a Benzothiadiazole-Cyclopentadithiophene Copolymer. *Adv. Mater.* **2013**, *25* (13), 1939–1947. https://doi.org/10.1002/adma.201201058.

(3) Cheng, C.; Geng, H.; Yi, Y.; Shuai, Z. Super-Exchange-Induced High Performance Charge Transport in Donor–Acceptor Copolymers. *J. Mater. Chem. C* **2017**, *5* (13), 3247–3253. https://doi.org/10.1039/C6TC05534F.

(4) Venkateshvaran, D.; Nikolka, M.; Sadhanala, A.; Lemaur, V.; Zelazny, M.; Kepa, M.; Hurhangee, M.; Kronemeijer, A. J.; Pecunia, V.; Nasrallah, I.; Romanov, I.; Broch, K.; McCulloch, I.; Emin, D.; Olivier, Y.; Cornil, J.; Beljonne, D.; Sirringhaus, H. Approaching Disorder-Free Transport in High-Mobility Conjugated Polymers. *Nature* **2014**, *515* (7527), 384–388. https://doi.org/10.1038/nature13854.

(5) Zhao, Y.; Truhlar, D. G. The M06 Suite of Density Functionals for Main Group Thermochemistry, Thermochemical Kinetics, Noncovalent Interactions, Excited States, and Transition Elements: Two New Functionals and Systematic Testing of Four M06-

Class Functionals and 12 Other Functionals. *Theor. Chem. Acc.* **2008**, *120* (1–3), 215–241. https://doi.org/10.1007/s00214-007-0310-x.

(6) Gaussian 16,Frisch, M. J.; Trucks, G. W.; Schlegel, H. B.; Scuseria, G. E.; Robb, M. A.; Cheeseman, J. R.; Scalmani, G.; Barone, V.; Petersson, G. A.; Nakatsuji, H.; Li, X.; Caricato, M.; Marenich, A. V.; Bloino, J.; Janesko, B. G.; Gomperts, R.; Mennucci, D. J. Gaussian 16. 2016.

(7) Fischer, F. S. U.; Trefz, D.; Back, J.; Kayunkid, N.; Tornow, B.; Albrecht, S.; Yager, K. G.; Singh, G.; Karim, A.; Neher, D.; Brinkmann, M.; Ludwigs, S. Highly Crystalline Films of PCPDTBT with Branched Side Chains by Solvent Vapor Crystallization: Influence on Opto-Electronic Properties. *Adv. Mater.* **2015**, *27* (7), 1223–1228. https://doi.org/10.1002/adma.201403475.

(8) Dolg, M.; Wedig, U.; Stoll, H.; Preuss, H. Energy-adjusted Abinitio Pseudopotentials for the First Row Transition Elements. *J. Chem. Phys.* **1987**, *86* (2), 866–872. https://doi.org/10.1063/1.452288.

(9) Yue, W.; Zhao, Y.; Shao, S.; Tian, H.; Xie, Z.; Geng, Y.; Wang, F. Novel NIR-Absorbing Conjugated Polymers for Efficient Polymer Solar Cells: Effect of Alkyl Chain Length on Device Performance. *J. Mater. Chem.* **2009**. https://doi.org/10.1039/b818885h.

(10) Zhu, Z.; Waller, D.; Gaudiana, R.; Morana, M.; Mühlbacher, D.; Scharber, M.; Brabec, C. Panchromatic Conjugated Polymers Containing Alternating Donor/ Acceptor Units for Photovoltaic Applications. *Macromolecules* **2007**, *40* (6), 1981–1986. https://doi.org/10.1021/ma062376o.

(11) Madsen, G. K. H.; Singh, D. J. BoltzTraP. A Code for Calculating Band-Structure Dependent Quantities. *Comput. Phys. Commun.* **2006**, *175* (1), 67–71. https://doi.org/http://dx.doi.org/10.1016/j.cpc.2006.03.007.

(12) Madsen, G. K. H. Automated Search for New Thermoelectric Materials: The Case of LiZnSb. *J. Am. Chem. Soc.* **2006**, *128* (37), 12140–12146. https://doi.org/10.1021/ja062526a.

(13) Jiang, H.; Shen, Y.-C. Ionization Potentials of Semiconductors from First-Principles. *J. Chem. Phys.* **2013**, *139* (16), 164114. https://doi.org/10.1063/1.4826321.